$$\frac{\partial^2 u}{\partial x^2} = 3\frac{d^2U}{dx^2}\left(-\frac{y}{a}+\frac{1}{2}\frac{y^2}{a^2}\right)+6\frac{dU}{dx}\frac{da}{dx}\left(\frac{y}{a^2}-\frac{y^2}{a^3}\right)$$
$$+3U\frac{d^2a}{dx^2}\left(\frac{y}{a^2}-\frac{y^2}{a^3}\right)+3U\left(\frac{da}{dx}\right)^2\left(-\frac{2y}{a^3}+\frac{3y^2}{a^4}\right)$$

$$\frac{\partial u}{\partial y} = 3\,U\left(-\frac{1}{a}+\frac{y}{a^2}\right)$$

$$\frac{\partial^2 u}{\partial y^2} = 3\,U/a^2$$

$$\frac{\partial p}{\partial x} = -\mu\left[\frac{\partial^2 u}{\partial x^2}+\frac{\partial}{\partial x}\left(\frac{\partial u}{\partial x}\right)_a\right]-\sigma\frac{d^3a}{dx^3}$$

Substituting the last expressions in Equation (13), and integrating with respect to y from zero to a, we get

$$\rho\left(\frac{9}{10}a\,U\frac{dU}{dx}-\frac{3}{10}U^2\frac{da}{dx}-a\,u_0\frac{dU}{dx}+\frac{u_0}{2}U\frac{da}{dx}\right)$$
$$=\sigma a\frac{d^3a}{dx^3}-\frac{7}{2}\mu a\frac{d^2U}{dx^2}+2\mu\frac{da}{dx}\frac{dU}{dx}+3\mu\frac{U}{a}-\rho\,ga$$
$$+\mu U\frac{d^2a}{dx^2} \quad \text{(A3)}$$

By using Equation (20), the constant flux condition along the meniscus can be expressed as

$$Q=\int_0^a u\,dy = a(x)\;[u_0-U(x)]$$

By using the last equation, the function $U(x)$ can be substituted in Equation (A3) by the function $a(x)$, and we get

$$\rho\left(\frac{u_0^2}{5}a^2\frac{da}{dx}-\frac{6}{5}Q^2\frac{da}{dx}\right)=\sigma a^3\frac{d^3a}{dx^3}+\left(\mu u_0 a^2\right.$$
$$\left.-\frac{9}{2}\mu Qa\right)\frac{d^2a}{dx^2}+9\mu Q\left(\frac{da}{dx}\right)^2+3\mu u_0 a-3\mu Q-\rho g a^3 \quad \text{(A4)}$$

By introducing the dimensionless variables

$$h=\frac{a}{a_0} \qquad \xi=\frac{x}{a_0}$$

Equation (A4) reduces to Equation (21).

Numerical Treatment of Laminar Flow in Helically Coiled Tubes of Square Cross Section

Part I. Stationary Helically Coiled Tubes

B. JOSEPH
E. P. SMITH
and
R. J. ADLER

Chemical Engineering Department
Case Institute of Technology
Case Western Reserve University
Cleveland, Ohio 44106

Numerical solutions of steady laminar flow in helically coiled tubes of square cross section for Dean numbers from 0.8 to 307.8 reveal two regimes of secondary flow. Up to Dean numbers of 100, the expected secondary flow pattern appears with twin counterrotating vortices. Above Dean numbers of 100, a new secondary flow regime, reported here for the first time, appears with four vortices. Flow visualization and pressure drop experiments confirm the transition.

SCOPE

When fluid flows through a helically coiled tube, centrifugal forces cause secondary flows, that is, currents in the cross-sectional plane. The fluid near the center of the tube, because it has the maximum downstream velocity, experiences the maximum centrifugal force and is thrown outward. Replacement fluid flows inward along the walls. A secondary flow pattern consisting of twin counterrotating vortices has been reported in all previous studies.

Helically coiled tubes often appear in process applications. Useful characteristics include, in addition to compactness, high rates of heat and mass transfer, enhanced cross-sectional mixing, low axial dispersion and an extended laminar flow regime—the transition from laminar to turbulent flow occurs at Reynolds numbers of 4,000 to 6,000 for typical geometries.

Most prior studies on helically coiled tubes have been for round cross sections. The only study of rectangular cross sections is an analytical solution limited to very low flow rates. However, rectangular cross sections arise in

Correspondence concerning this paper should be addressed to R. J. Adler.

certain applications. For example, in jacketed kettles or concentric cylinders with membrane walls, the annular region between two cylinders often contains a spiraling spacer which, together with the cylinder walls, forms a helically coiled tube with rectangular cross section. Another example is a spiral-cut fin tube inside a concentric, close-fitting smooth tube.

This work studies secondary flows in helically coiled tubes of square cross section. The primary objective is to determine whether the twin counterrotating vortices always observed heretofore occur when the cross section is square.

Using finite difference techniques, the Navier Stokes and continuity equations are solved on the computer for seven Dean numbers from 0.8 to 307.8. Axial velocity profiles, secondary flows in the cross-sectional plane, and pressure distributions are determined for steady state, fully developed flow. Supplementary flow visualization and pressure drop experiments are performed to confirm the main characteristics of the computed solutions.

CONCLUSIONS AND SIGNIFICANCE

At low flow rates up to a Dean number of 100, twin counterrotating vortex secondary flow patterns are obtained. This secondary flow pattern is of the type reported by investigators in all previous work. At a Dean number of 100, an abrupt transition occurs to a new secondary flow pattern of four vortices. All four vortices are of similar strength, but are unequal in size.

The finding of a new secondary flow pattern with four vortices suggests that cross-sectional shape may have a larger influence on secondary flow than previously believed. Applications are likely where secondary flow effects, which depend on cross-sectional mixing, may be enhanced by switching back and forth between the two laminar flow regimes by varying the Dean number from just below to just above 100.

BACKGROUND

The literature describing secondary flow in helically coiled tubes dates back to the beginning of the century. Most prior investigations have studied coils of round cross section. For round cross sections Dean (1927, 1928) solved the Navier-Stokes equations analytically in laminar flow for large radii of curvature of the helix. He found secondary flow is characterized by a dimensionless parameter called the Dean number $N_{De} = N_{Re}(a/r)^{1/2}$, where a is the radius of the pipe and r is the radius of the helix. Dean's analytical solution, valid for $N_{De} < 1$, shows twin counterrotating currents in the cross-sectional plane. Numerical solutions by Truesdell and Adler (1970) and Austin and Seader (1973), valid for $N_{De} \leq 100$ and $N_{De} \leq 1000$, respectively, show twin counterrotating secondary currents at higher Dean numbers. Experimental observations by numerous investigators (Eustice, 1911; Taylor, 1929; Koutsky and Adler, 1964) confirm that twin rotating currents occur at all Dean numbers in round helical tubes.

Helically coiled tubes of nonround cross section have been investigated less intensely. Cuming (1952) applied Dean's analytical approach to rectangular and elliptical cross sections. Cuming's solutions, valid for $N_{De} < 1$, again show twin rotating currents in the cross-sectional plane. Truesdell and Adler's (1970) finite difference solution for elliptical cross section, valid for $N_{De} < 100$, also shows twin rotating currents.

Thus, all previous studies of flow in helically coiled tubes have reported a single regime of secondary flow in the cross section, namely, twin counterrotating vortices.

EQUATIONS OF MOTION

The continuous Navier-Stokes and continuity equations are developed.

Consider a tube with square cross section wound into a helix on a round, cylindrical mandrel. Except near the entrance and the exit of the tube, the flow will be fully developed and independent of downstream position. For small angles of pitch, the geometry of a torus is a good approximation. Truesdell and Adler (1970) have shown that the major effect of a finite pitch can be taken into account by modifying the radius of curvature. The right-handed orthogonal coordinate system used in the torus approximation is shown in Figure 1.

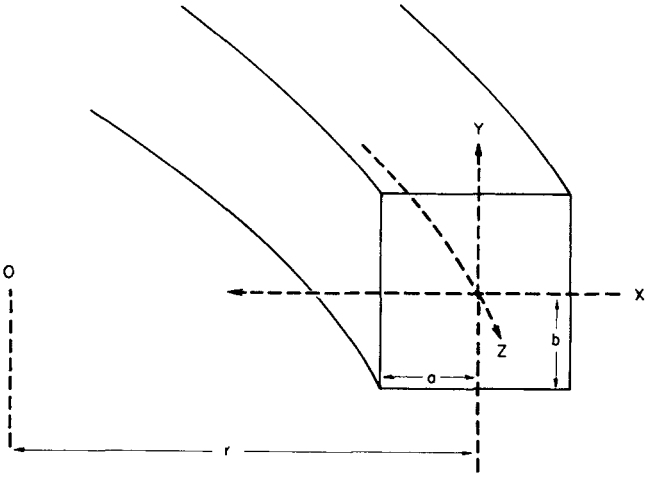

Fig. 1. Coordinate system.

The equations of motion for laminar, fully developed, isothermal, Newtonian flow have been stated in dimensionless form by Cuming (1952). The dimensionless variables are defined as follows: The velocities u, v, w in the X, Y, Z directions are related to dimensionless velocities U, V, W by $u = \frac{\nu U}{a}$, $v = \frac{\nu V}{a}$ and $w = \frac{\nu W}{a}$, where ν is the kinematic viscosity of the fluid. Lengths are nondimensionalized by $x = aX$, $y = a\lambda Y$, $z = aZ$ where $\lambda = b/a$. The pressure p is related to the dimensionless pressure P by $p = \rho\nu^2 P/a^2$. Time t is related to dimensionless time T by $t = \frac{a^2 T}{\nu}$. The equations of motion are

$$\frac{\partial U}{\partial T} = -U\frac{\partial U}{\partial X} - \frac{V}{\lambda}\frac{\partial U}{\partial Y} + \frac{(a/r)W^2}{\left(1+\frac{a}{r}X\right)} - \frac{\partial P}{\partial X} + \frac{1}{\lambda^2}\frac{\partial^2 U}{\partial Y^2} - \frac{1}{\lambda}\frac{\partial^2 V}{\partial X \partial Y} \quad (1a)$$

$$\frac{\partial V}{\partial T} = -U\frac{\partial V}{\partial X} - \frac{V}{\lambda}\frac{\partial V}{\partial Y} - \frac{1}{\lambda}\frac{\partial P}{\partial Y} + \frac{\partial^2 V}{\partial X^2}$$

$$-\frac{1}{\lambda}\frac{\partial^2 U}{\partial X \partial Y}+\frac{(a/r)}{[1+(a/r)X]}\left(\frac{\partial V}{\partial X}-\frac{1}{\lambda}\frac{\partial U}{\partial Y}\right) \quad (1b)$$

$$\frac{\partial W}{\partial T}=-U\frac{\partial W}{\partial X}-\frac{V}{\lambda}\frac{\partial W}{\partial Y}-\frac{(a/r)UW}{[1+(a/r)X]}$$
$$-\frac{1}{[1+(a/r)X]}\frac{\partial P}{\partial Z}+\frac{\partial^2 W}{\partial X^2}+\frac{1}{\lambda^2}\frac{\partial^2 W}{\partial Y^2}$$
$$+\frac{(a/r)}{[1+(a/r)X]}\frac{\partial W}{\partial X}-\frac{(a/r)^2 W}{[1+(a/r)X]^2} \quad (1c)$$

and the equation of continuity is

$$\frac{\partial}{\partial X}[1+(a/r)X]\,U+\frac{1}{\lambda}\frac{\partial}{\partial Y}[1+(a/r)X]\,V=0 \quad (1d)$$

Because the flow is symmetrical about the X-axis, a solution is required only in the upper or lower half-plane. In this work a solution is obtained in the upper half-plane.

The boundary conditions are no slip along the walls, that is,

$$\left.\begin{aligned}U&=0\\V&=0\\W&=0\end{aligned}\right\}\ \text{on the wall boundary,}$$

and symmetry with respect to the X-axis, that is,

$$\left.\begin{aligned}\frac{\partial U}{\partial Y}&=0\\V&=0\\\frac{\partial W}{\partial Y}&=0\end{aligned}\right\}\ \text{along } Y=0.$$

A stream function ψ for the velocities U and V in the cross-sectional plane is defined by

$$V=\frac{-1}{(1+(a/r)X)}\frac{\partial \psi}{\partial X}$$

$$U=\frac{1}{\lambda(1+(a/r)X)}\frac{\partial \psi}{\partial Y}$$

While all the computations were performed in the primitive variables, that is, the velocities and pressure, the results of the secondary flows are reported in terms of the stream function for convenience of visualization. The equations used to compute the stream function from the velocities are developed and reported in Appendix I* of Joseph (1974).

DISCRETE EQUATIONS

The numerical method employed here is similar to the Marker-and-Cell method suggested by Harlow and Welch (1964), the essential difference being in the formulation of the equation for pressure and in the placement of the velocity and pressure nodes. The particular configuration used in this work was chosen to avoid extrapolating velocities and pressures beyond the boundary.

The entire region above the X-axis is divided into a 20 × 10 mesh with each cell 0.1 × 0.1 in size (dimensionless) (see Figure 2). This choice of mesh size is based on

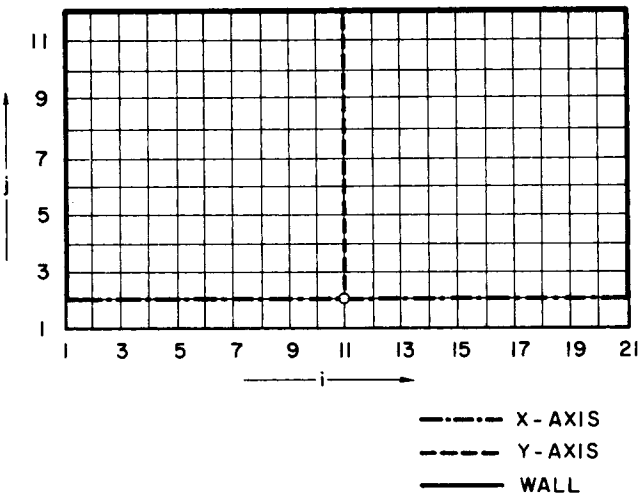

Fig. 2. Grid.

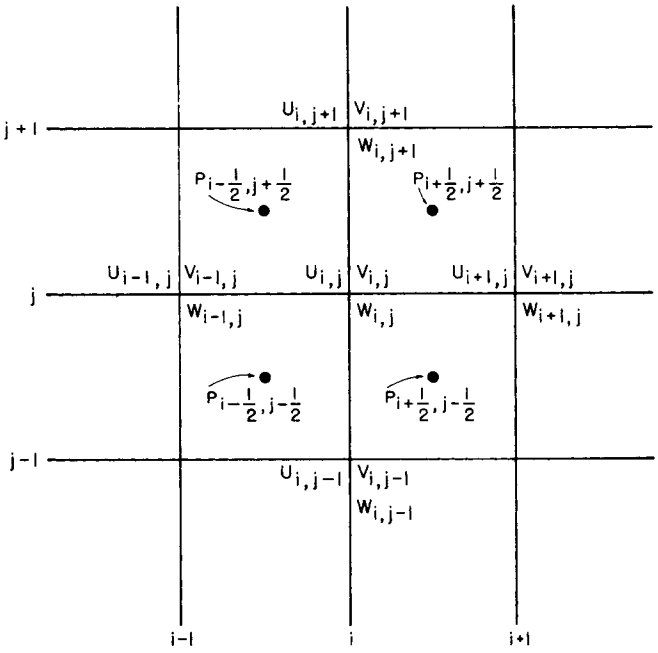

Fig. 3. Velocity and pressure nodes.

work by previous investigators in the field (Truesdell and Adler, 1970; Austin and Seader, 1973). The velocities are defined at cell corners with subscript i representing X-position and j representing Y-position. The origin ($X = 0$, $Y = 0$) is identified as $i = 11$, $j = 2$. Pressures are defined at cell centers and have half integer indices (see Figure 3).

Finite-Differenced Momentum and Continuity Equations

The momentum and continuity equations were finite differenced as follows. The time derivative terms in the momentum equations (1a), (1b), and (1c) were replaced by first-order forward differences. The first derivative with respect to the X and Y space coordinates were replaced by second-order central differences and the diffusion term was replaced by a second-order approximation similar to the Dufort-Frankel scheme (1953). The pressure derivative was replaced by a four point, first-order approximation. The finite differenced versions of (1a), (1b), and (1c) are:

$$\frac{U_{ij}^{n+1}-U_{ij}^{n}}{\Delta T}=-U_{ij}^{n}\frac{U_{i+1,j}^{n}-U_{i-1,j}^{n}}{2\Delta X}$$

* Appendices I to V are contained in the Supplement which has been deposited as Document No. 02671 with the National Auxiliary Publications service (NAPS), c/o Microfiche Publications, 440 Park Ave. South, N.Y., N. Y. 10016 and may be obtained for $1.50 for microfiche or $5.00 for photocopies.

$$- V_{ij}\frac{U^n_{i,j+1} - U^n_{i,j-1}}{2\lambda\Delta Y} + \frac{A}{B_i}(W^n_{ij})^2$$

$$+ \frac{U^n_{i,j+1} - U^{n+1}_{ij} - U^{n-1}_{ij} - U^n_{i,j-1}}{2(\Delta Y)^2\lambda^2}$$

$$- \frac{V^n_{i+1,j+1} - V^n_{i-1,j+1} - V^n_{i+1,j-1} + V^n_{i-1,j-1}}{4\lambda\Delta X\Delta Y}$$

$$- \frac{P^{n+1}_{i+\frac{1}{2},j+\frac{1}{2}} + P^{n+1}_{i+\frac{1}{2},j-\frac{1}{2}} - P^{n+1}_{i-\frac{1}{2},j+\frac{1}{2}} - P^{n+1}_{i-\frac{1}{2},j-\frac{1}{2}}}{2\Delta X} \qquad (2a)$$

$$\frac{V^{n+1}_{ij} - V^n_{ij}}{\Delta T} = - U^n_{ij}\frac{V^n_{i+1,j} - V^n_{i-1,j}}{2\Delta X}$$

$$- V^n_{ij}\frac{V^n_{i,j+1} - V^n_{i,j-1}}{\lambda\Delta Y} + \frac{A}{B_i}\left[\frac{V^n_{i+1,j} - V^n_{i-1,j}}{2\Delta X}\right.$$

$$\left. - \frac{U^n_{i,j+1} - U^n_{i,j-1}}{2\lambda\Delta Y}\right]$$

$$+ \frac{V^n_{i+1,j} - V^{n+1}_{i,j} - V^{n-1}_{i,j} + V^n_{i-1,j}}{(\Delta X)^2}$$

$$- \frac{U^n_{i+1,j+1} - U^n_{i-1,j+1} - U^n_{i+1,j-1} + U^n_{i-1,j-1}}{4\lambda\Delta X\,\Delta Y}$$

$$- \frac{P^{n+1}_{i+\frac{1}{2},j+\frac{1}{2}} + P^{n+1}_{i-\frac{1}{2},j+\frac{1}{2}} - P^{n+1}_{i+\frac{1}{2},j-\frac{1}{2}} - P^{n+1}_{i-\frac{1}{2},j-\frac{1}{2}}}{2\lambda\Delta Y} \qquad (2b)$$

$$\frac{W^{n+1}_{ij} - W^n_{ij}}{\Delta T} = - U^{n+1}_{ij}\frac{W^n_{i+1,j} - W^n_{i-1,j}}{2\Delta X}$$

$$- V^{n+1}_{ij}\frac{W^n_{i,j+1} - W^n_{i,j-1}}{2\lambda\Delta Y} - \frac{A}{B_i}U^{n+1}_{ij}W^n_{ij}$$

$$- \frac{1}{B_i}\frac{\partial P}{\partial Z} + \frac{A}{B_i}\frac{W^n_{i+1,j} - W^n_{i-1,j}}{2\Delta X}$$

$$- \frac{A^2}{(B_i)^2}W^n_{ij} + \frac{W^n_{i+1,j} - W^{n+1}_{ij} - W^{n-1}_{ij} + W^n_{i-1,j}}{(\Delta X)^2}$$

$$+ \frac{W^n_{i,j+1} - W^{n+1}_{ij} - W^{n-1}_{ij} + W^n_{i,j-1}}{\lambda^2(\Delta Y)^2} \qquad (2c)$$

The continuity equation is finite differenced at the cell center; time level $n + 1$ is used for later convenience.

$$\frac{(U^{n+1}_{i+1,j+1} + U^{n+1}_{i+1,j})\,B_{i+1} - (U^{n+1}_{i,j+1} + U^{n+1}_{ij})B_i}{2\Delta X}$$

$$+ \frac{(V^{n+1}_{i+1,j+1} + V^{n+1}_{i,j+1} - V^{n+1}_{i+1,j} - V^{n+1}_{ij})}{2\lambda Y\Delta}B_{i+1/2} = 0 \qquad (2d)$$

This particular form of finite-differencing was chosen in part so that the continuity equation could be satisfied easily.

Equations (2a) and (2b) are solved explicitly for $U_{i,j}{}^{n+1}$ and $V_{i,j}{}^{n+1}$ and these expressions are substituted into Equation (2d) to obtain a relation between the pressures at time $n + 1$ and the velocities at time n. This relation is referred to as the auxiliary pressure equation. See Appendix II* for the detailed development of the auxiliary pressure equation.

Equations (2a), (2b), (2c) and the auxiliary pressure equation describe the (discrete) time dependent behavior of the fluid. A steady state solution is obtained by using these four equations to advance the velocities and pressure from one time interval to another until the solution no longer changes with time. The order in which these calculations are carried out is explained in the section on Solution Procedure. A simplified linear stability analysis of these equations is given in Appendix III.*

Boundary and Initial Conditions

Since the mesh coincides with the boundary, the velocity at the grid points along the boundary are known at all times. This information is also used in deriving the auxiliary equation for pressure near the boundary so that extrapolation beyond the boundary is avoided. This is illustrated by an example. Consider the continuity equation written at cell centers adjacent to the left wall ($Y = -1$):

$$\frac{(U^{n+1}_{2,j} + U^{n+1}_{2,j+1})\,B_2 - (U^{n+1}_{1,j+1} - U^{n+1}_{1,j})\,B_1}{2\Delta X}$$

$$+ \frac{(V^{n+1}_{2,j+1} + V^{n+1}_{1,j+1} - V^{n+1}_{2,j} - V^{n+1}_{1,j})\,B_{1+1/2}}{2\lambda\Delta Y} = 0 \qquad (3a)$$

From the boundary conditions on U and V we have $U_{1,j} = 0$, $V_{1,j} = 0$. Hence the equation simplifies to

$$\frac{(U^{n+1}_{2,j} + U^{n+1}_{2,j+1})\,B_2}{2\Delta X} + \frac{(V^{n+1}_{2,j+1} - V^{n+1}_{2,j})}{2\lambda\Delta Y}B_{1+1/2} = 0 \qquad (3b)$$

Now the expressions for the velocities at time $n + 1$ at the interior points as defined by (2a) and (2b) can be substituted in the above equation to obtain the equation for pressure near the boundary. Similar treatments apply at other boundaries and near the corners. Along the X-axis, the condition $\partial P/\partial Y = 0$ applies. This is incorporated by substituting $P^{n+1}_{i+\frac{1}{2},\frac{1}{2}} = P^{n+1}_{i+\frac{1}{2},1+\frac{1}{2}}$ wherever the first quantity appears. Thus the pressures below the X-axis do not enter into the iterative solution. This method of treatment near the X-axis aided the convergence of the iterative procedure for solving the pressure equation. Another method which used pressure variables below the X-axis in the iterative procedure led to diverging solutions for pressure.

See Appendix II* for a complete listing of the boundary pressure equations.

At the beginning of each run, the initial velocities were set equal to the converged velocities from a prior run at the same radius of curvature for the nearest Dean number previously calculated. If such a converged solution was not available, the initial velocities were set to zero.

* See footnote on page 967.

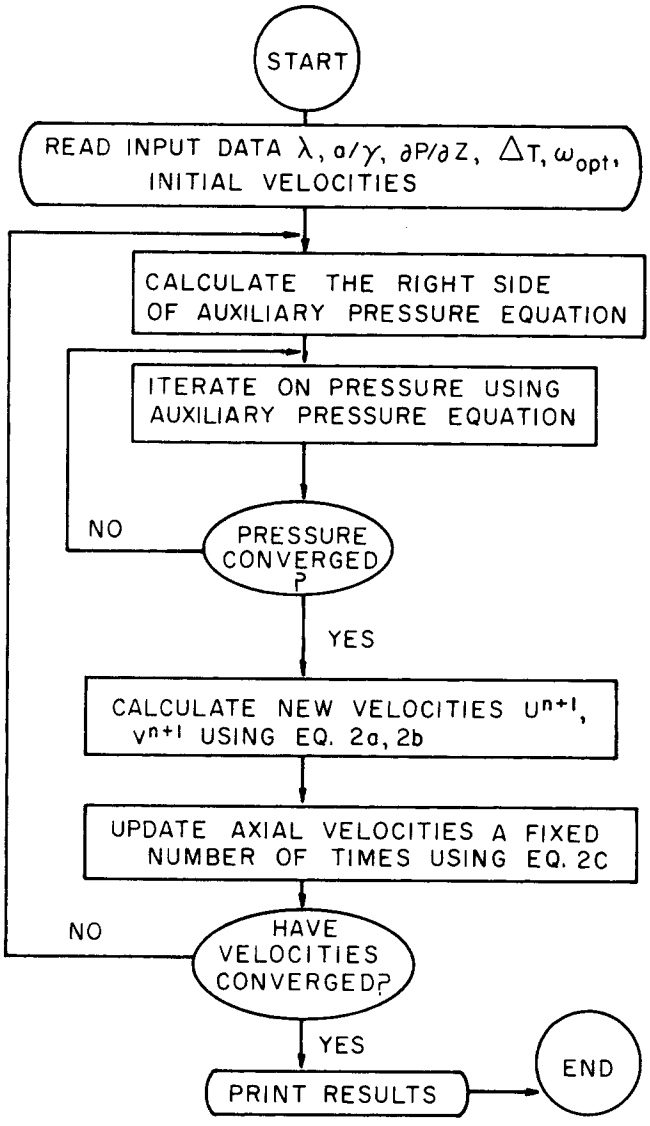

Fig. 4. Flow chart.

SOLUTION PROCEDURE

Since 60 to 80% of the computing time is used in calculating the pressure, it was necessary to use an efficient algorithm to solve the simultaneous linear equations in pressure. They were solved by the optimum successive over-relaxation method (Young, 1954). The optimum over-relaxation factors were determined by numerical experimentation following the method outlined by Carré (1961). After the pressures converged, a constant was added to the converged values of pressure so that the pressure at the origin was arbitrarily made zero. (Adding a constant does not change the pressure gradient.)

The flow chart of the computer program is shown in Figure 4. At the beginning of each iteration in time, the right-hand side of the auxiliary pressure equation is calculated and stored. The pressure is calculated next by iteration, until the change in successive iterates of pressure is smaller than a preset quantity, say ϵ, which determines how accurately the continuity equation will be satisfied. The velocities are updated next. Convergence of the velocities was more difficult to determine since they exhibited small amplitude oscillations after reaching the neighborhood of the expected steady state solution. Convergence of the velocities was assumed when the amplitude of oscillations became less than 1% of the expected value. These oscillations were considerably reduced, and the rate of overall convergence increased, by iterating on the axial velocities several times during every time step as indicated in the flow chart. The effectiveness of this internal iteration procedure is related to the coupling between the three momentum equations. A similar procedure was employed by Austin and Seader (1973).

The calculations were performed on a UNIVAC 1108 computer. Between 50 and 250 time iterations were required for the velocities to converge; about a second of computer time was required for each of these time iterations. Within each time iteration about thirty iterations were used on the average to converge the pressures. The timestep used varied from 0.01 to 0.0005. The number of time iterations needed to obtain convergence increased as the Dean number increased.

RESULTS

Seven runs were made at different axial pressure gradients and curvature ratios. See Table 1. The Dean number ranged from 0.788 to 307.83. Two different types of flow patterns were observed.

At low Dean numbers twin counterrotating secondary vortices of the type reported by investigators in all previous work were obtained. Runs 1, 2, 3, and 4 with Dean numbers from 0.788 to 94.57 show these usual twin rotating currents. See Figures 5, 6, and 7. The results for Run 2 are reported in Appendix V.*

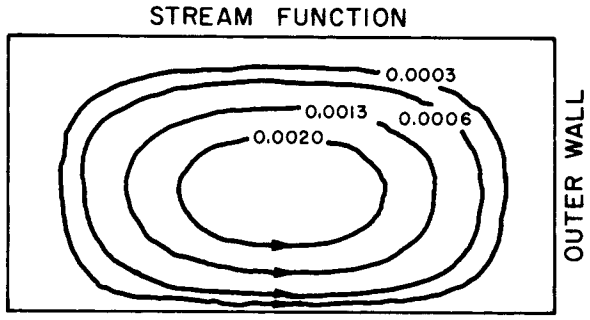

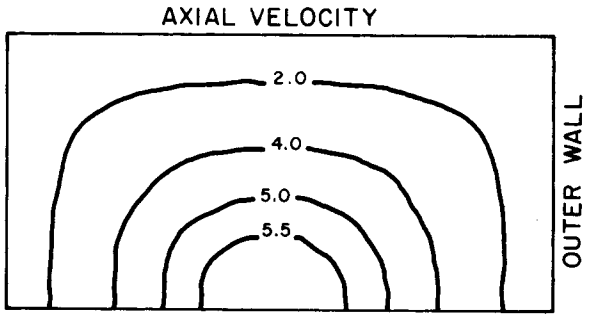

N_{De} = .788 $\quad \frac{a}{r}$ = 0.02 $\quad \frac{\partial P}{\partial Z}$ = −20.0

N_{Re} = 5.58

Fig. 5. Run 1, stream function and axial velocity.

* See footnote on page 967.

TABLE 1. COMPUTED SOLUTIONS FOR STATIONARY HELIX

Run no.	Fig. no.	$\frac{\partial P}{\partial Z}$	a/r	N_{Re}*	N_{De}**	fs/fc***	ΔP_D	Initial velocity conditions	No. of time iterations
1	5	−20.0	.02	5.577	.788	1.0000	.618	Zero	63
2	V-1‡	−800.0	.01	208.42	20.842	1.0700	425.9	Zero	50
3	6	−800.0	.05	181.86	40.66	1.2260	1,496.3	Zero	80
4	7	−1,600.0	.01	299.06	94.57	1.4919	6,426.0	Results of Run 2	180
5	8	−2,000.0	.01	339.36	107.36	1.6427	7,586.8	Results of Run 4	167
6	9	−8,000.0	.05	1,090.8	243.91	2.045	38,818.7	Results of Run 3	250
7†	10	−8,000.0	.10	973.4	307.83	2.2916	61,088.0	Zero	280

* Based on hydraulic radius, R_h.

** $N_{De} = N_{Re} \times \sqrt{a/r}$.

*** Flux through a straight tube at the same pressure drop divided by the flux through the helix.

† Solution only approximate. Complete convergence not obtained because of weakly damped oscillations.

‡ See Appendix V.

At higher Dean numbers four secondary vortices, counterrotating in pairs, are present. Runs 5, 6, and 7 with Dean numbers from 107.36 to 307.83 show these unusual secondary flow patterns. See Figures 8, 9, and 10. The additional pair of rotating vortices are located near the outer wall in symmetrical positions above and below the X-axis. The normal twin counterrotating secondary vortices are also present but are distorted to accommodate the additional pair of vortices While the additional rotating vortices are smaller than the normal rotating currents, they are equally as strong in terms of velocities.

The transition from two to four rotating vortices is associated with a progressive shifting of the axial velocity peak toward the outer wall, and a progressive flattening of the axial velocity profile, as the Dean number is increased. In the neighborhood of a Dean number of 100, the axial velocity profile inverts at the point of maximum axial velocity; the location of the former axial velocity peak becomes the location of a local minimum in axial velocity. Thus, there is a region near the outer wall where the axial velocity is greater above and below the X-axis than on the X-axis. Centrifugal forces act most strongly on the fluid moving downstream fastest; hence the additional rotating currents appear.

The results were checked for uniqueness by starting with different initial conditions. In particular, the existence of the four vortex regime was further confirmed by solving the problem using a different numerical scheme

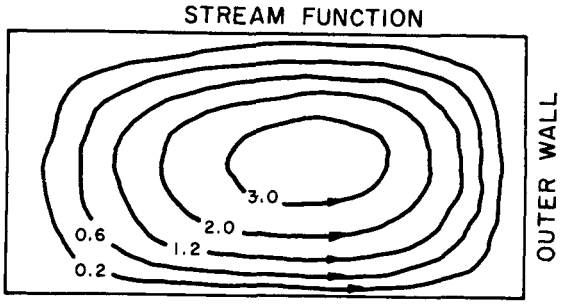

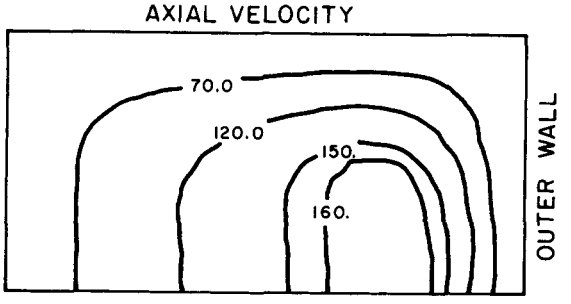

N_{De} = 40.66 $\frac{a}{r}$ = 0.05 $\frac{\partial P}{\partial Z}$ = −800.0

N_{Re} = 181.86

Fig. 6. Run 3, stream function and axial velocity.

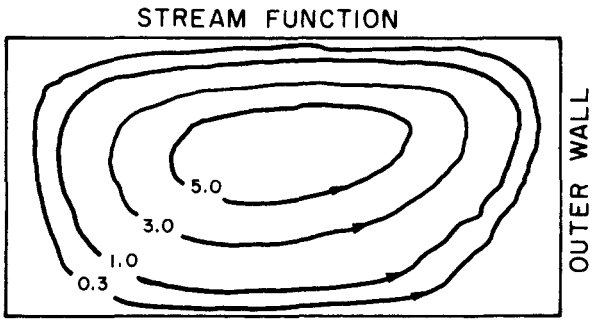

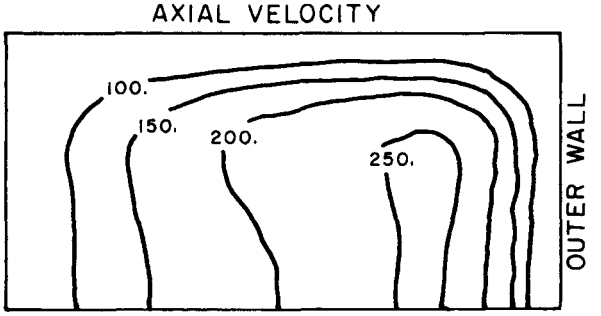

N_{De} = 94.57 $\frac{a}{r}$ = 0.01 $\frac{\partial P}{\partial Z}$ = −1600.

N_{Re} = 299.06

Fig. 7. Run 4, stream function and axial velocity.

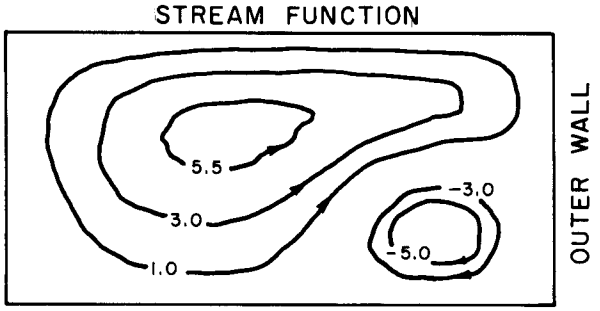

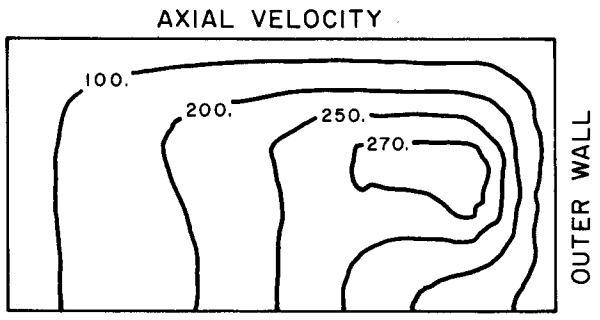

N_{De} = 107.36 $\frac{a}{r}$ = 0.01 $\frac{\partial P}{\partial Z}$ = − 2000.

N_{Re} = 339.51

Fig. 8. Run 5, stream function and axial velocity.

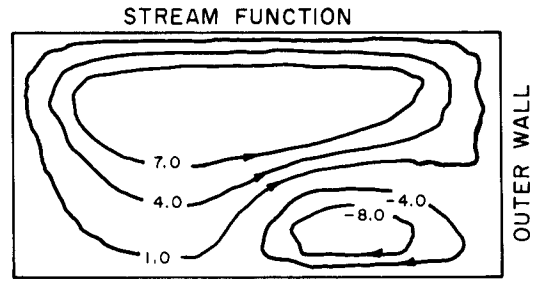

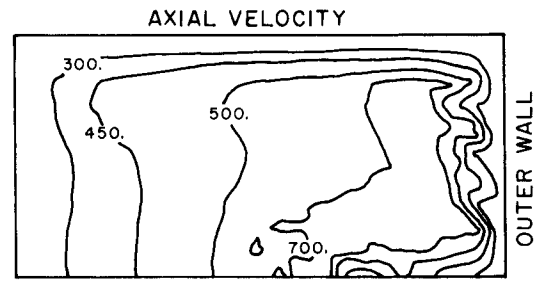

N_{De} = 307.83 $\frac{a}{r}$ = 0.10 $\frac{\partial P}{\partial Z}$ = − 8000.0

N_{Re} = 973.468

Fig. 10. Run 7, stream function and axial velocity.

proposed by Chorin (1968). In Chorin's formulation, the velocities and pressure are defined at the same points along

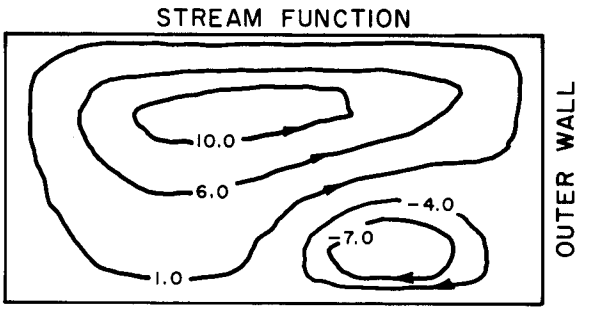

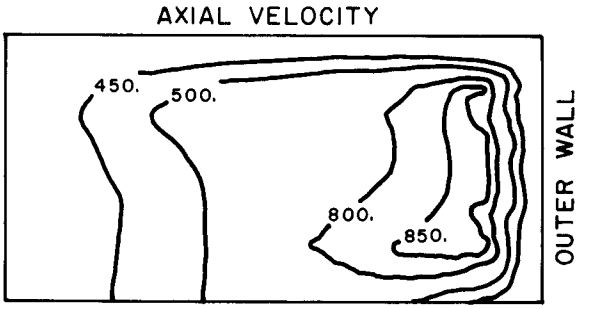

N_{De} = 243.91 $\frac{a}{r}$ = 0.05 $\frac{\partial P}{\partial Z}$ = − 8000.0

N_{Re} = 1090.79

Fig. 9. Run 6, stream function and axial velocity.

the mesh. Near the boundary the continuity equation is finite differenced in a one-sided manner to avoid extrapolation to points outside the boundary. Chorin first solved for auxiliary velocities U_{ij}^* and V_{ij}^* from the finite differenced momentum equations after deleting the pressure derivatives. The velocities at time $n + 1$ are defined as follows:

$$U_{ij}^{n+1} = U_{ij}^* - \frac{P_{i+1,j}^{n+1} - P_{i-1,j}^{n+1}}{2\Delta X} \Delta T \qquad (4a)$$

$$V_{ij}^{n+1} = V_{ij}^* - \frac{P_{i,j+1}^{n+1} - P_{i,j-1}^{n+1}}{2\Delta Y} \Delta T \qquad (4b)$$

These expressions are substituted into the finite differenced continuity equation to obtain Chorin's Poisson equation for pressure. This equation is formally less accurate than the Poisson equation used in this work. [Truncation errors $(2\Delta X)^2$ and $(\Delta X)^2$ respectively.] In addition, Chorin's method proved to be more oscillatory especially at higher Dean numbers. For Run 1, the converged steady state solution obtained using Chorin's method differed by about 2% from the solution reported.

A further check on the validity of the computer program was made by comparing the axial velocities calculated in Run No. 1 against the analytical solution for the axial velocities in a straight tube of square cross section. This comparison is appropriate since the axial velocity profile in a helically coiled tube at a Dean number of less than one is virtually unchanged from the axial velocity profile in a straight tube. Over most of the cross section, the axial velocity calculated from the computer program and the analytical solution agreed to within 1%.

An attempt was made to compare the results of this work at low Dean numbers with the analytical solution

of Cuming (1952). However, this was not possible because Cuming's approximate solution was found not to satisfy the full set of boundary conditions. See Appendix IV.*

All solutions exhibited damped oscillations about the steady state. Convergence was judged by the amplitude of these oscillations. In all runs, except Run number 7, the solution converged to steady state in 250 or fewer iterations. However, the velocities in Run 7 exhibited oscillations with amplitudes as high as 10% of the expected steady state values even after 300 iterations. These oscillations could not be avoided by taking smaller time steps. It is believed that a smaller space mesh is required to avoid these oscillations. This belief is based on the fact that oscillatory solutions are obtained for the one-dimensional diffusion-convection equation central differenced in space even with time continuous unless the spatial mesh is small enough (Price et al., 1966).

Figure 11 compares the flux diminution in the square helix with that in a circular helix. The flux diminution is defined as f_s/f_c, where f_c is the flux through a helix and f_s is the flux through a straight tube when subjected to the same axial pressure gradient as the helix. White (1929) has shown that the pressure drop through helices of circular cross section is well correlated by the Dean number. For the same Dean number, the flux diminution in a square helix is higher, a result not too surprising since the secondary flow in square helices is stronger. Figure 12 shows that the diametrical pressure drop, the pressure drop measured from the inner wall to the outer wall along the X-axis, is also higher in square helices than in circular helices.

EXPERIMENTAL CONFIRMATION

To confirm the calculated transition at a Dean number of 100 from two to four rotating vortices, flow visualization and pressure drop experiments were performed. The experiments are described in some detail because they lend credibility to the computed results.

A helically coiled tube of square cross section was constructed from clear acrylic plastic. The inner and outer

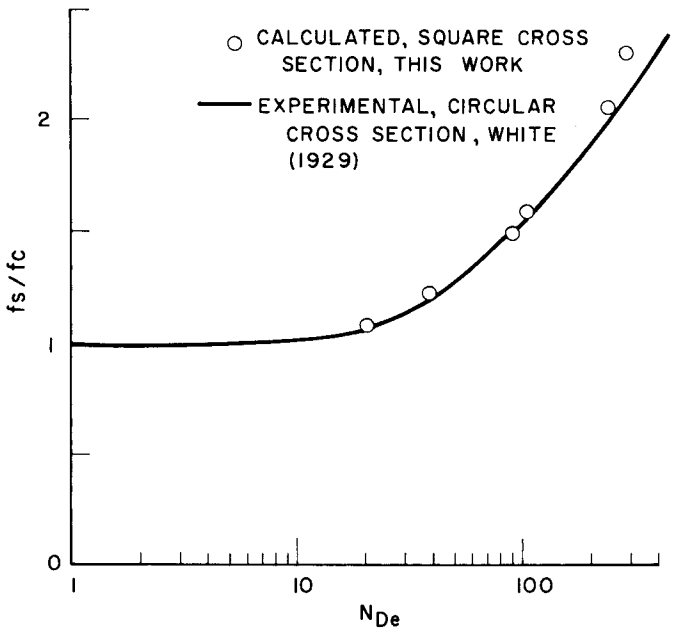

Fig. 11. Flux diminution.

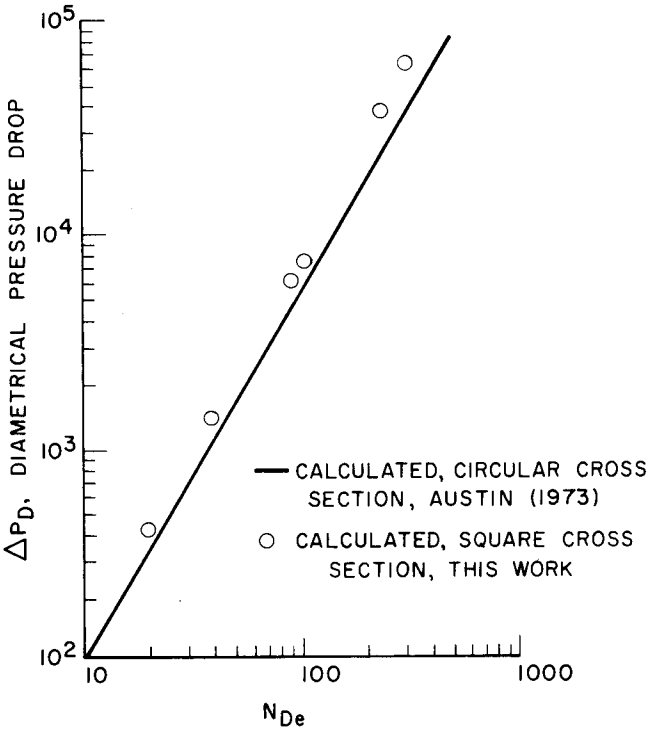

Fig. 12. Diametrical pressure drop.

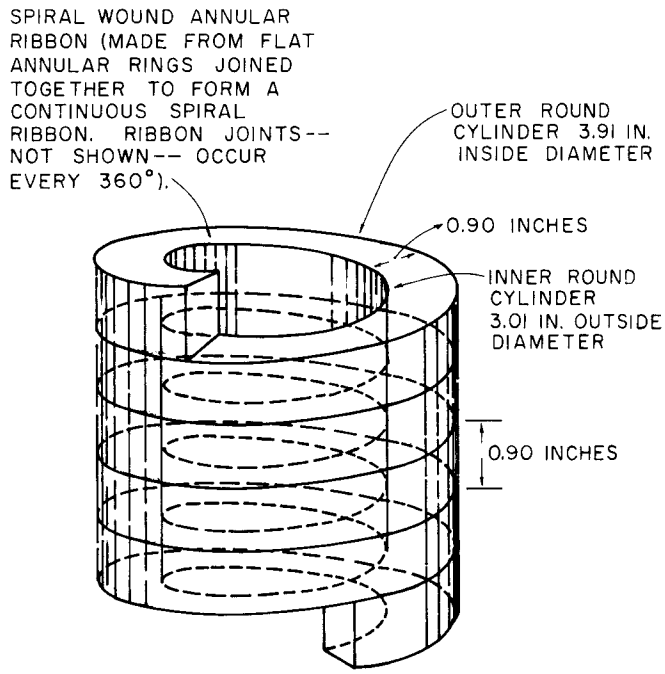

Fig. 13. Helically coiled tube of square cross section.

(curved) walls were two concentric cylinders. The top and bottom (flat) walls were made from washer-shaped pieces of sheet plastic, each with a single radial cut, joined together to make a continuous spiral or coil-spring shape. See Figure 13 (helically coiled tube of square cross section). The dimensions are:

Cross section	0.90 in. sq.
Radius of helix	3.46 in. (measured from the axis of the helix to the center of the square cross section).
Pitch	1.03 in. (distance measured parallel to helix axis between corresponding cross sectional positions on two successive wraps of the helically coiled tube).

* See footnote on page 967.

Water at room temperature flowed through the helically coiled tube at Dean numbers from 30 to 180. Dye tracer (dilute ink) was injected through a small section of rubber sheet in the outer wall of one coil in order to observe the flow patterns. The pressure drop was measured using manometers.

The flow visualization tracer studies revealed two regimes of laminar flow, with a transition at $N_{De} = 100$ ($\pm 5\%$ experimental accuracy). For $N_{De} < 100$, the flow is of the type previously observed in helically coiled tubes of round cross section, that is, twin rotating cells as shown in Figure 5. When a sufficient quantity of tracer was injected at one time to fill the cross section, the tracer was observed to form twin peaks as it flowed downstream, with the points of the peaks symmetrically located in the upper and lower half planes of the cross section. For $N_{De} > 100$ the twin rotating cells were accompanied by additional swirling patterns near the outer face of the cross section. In addition, when sufficient tracer was injected at one time to fill the cross section, the axial dispersion of the tracer as it flowed downstream was noticeably diminished for $N_{De} > 100$ when compared to the axial dispersion for $N_{De} < 100$.

When pressure drop was plotted as a function of N_{De}, there was a more rapid change in slope in the range $N_{De} = 85$ ($\pm 10\%$ experimental accuracy) to 105 ($\pm 10\%$ experimental accuracy) than for $N_{De} < 85$ or $N_{De} > 105$.

Although the experiments described were not sufficiently quantitative to check the details of the flow, they confirm that a transition occurs in the flow at $N_{De} = 100$ ($\pm 10\%$) and that the main features of the secondary flow are as calculated.

It should be noted that the curvature ratio a/r had a much different value in the experiments and calculations. The computed transition was for $a/r = 0.01$. The experimental transition was for $a/r = 0.130$. Thus, taken together, the computed and experimental results suggest that the transition criterion $N_{De} = 100$ is likely valid over an extended range of curvature ratios.

ACKNOWLEDGMENT

Financial support by the National Science Foundation, Grant GK 33818, is gratefully acknowledged.

NOTATION

a = half the width of the rectangular cross section in the X-direction, for circular tubes this is the radius of the cross section

A = dimensionless curvature $= (a/r)$

b = half the height of the rectangular cross section measured in the Y-direction, equal to a for square helices

B_i = a function, $1 + (a/r)X_i$

D_X = short notation for $\dfrac{1}{\Delta T} + \dfrac{1}{\lambda^2(\Delta Y)^2}$

D_Y = short notation for $\dfrac{1}{\Delta T} + \dfrac{1}{(\Delta X)^2}$

f_c = dimensionless flux through a curved pipe

f_s = dimensionless flux through a straight pipe

N_{De} = Dean number $= N_{Re}\sqrt{a/r}$

N_{Re} = Reynolds number based on hydraulic radius $= \dfrac{4R_h \rho \overline{W}}{\mu}$

p = pressure

P = dimensionless pressure $= a^2p/\rho\nu^2$

P_X = finite-differenced pressure gradient in the X-direction $= (P_{i+\frac{1}{2},j+\frac{1}{2}} + P_{i+\frac{1}{2},j-\frac{1}{2}} - P_{i-\frac{1}{2},j+\frac{1}{2}} - P_{i-\frac{1}{2},j-\frac{1}{2}})/(2\Delta X)$

P_Y = finite differenced pressure gradient in Y-direction [see Equation (2b)] $= (P_{i+\frac{1}{2},j+\frac{1}{2}} + P_{i-\frac{1}{2},j+\frac{1}{2}} - P_{i+\frac{1}{2},j-\frac{1}{2}} - P_{i-\frac{1}{2},j-\frac{1}{2}})/(2\lambda\Delta Y)$

R_h = hydraulic radius $= \dfrac{\text{cross-sectional area}}{\text{wetted perimeter}}$

r = radius of curvature of helix (see Figure 1)

t = time

T = dimensionless time $= t\nu/a^2$

u = velocity in X-direction

U = dimensionless velocity in X-direction $= a\rho u/\mu$

$\hat{U}$ = an auxiliary velocity defined by Equation (II-1a) in Appendix II

U^* = an auxiliary velocity defined by Equation (4a)

v = velocity in Y-direction

V = dimensionless velocity in Y direction $= a\rho v/\mu$

$\hat{V}$ = an auxiliary velocity defined by Equation (II-1b) in Appendix II

V^* = an auxiliary velocity defined by Equation (4b)

w = velocity in Z-direction

W = dimensionless velocity in Z-direction $= a\rho w/\mu$

$\overline{W}$ = average dimensionless velocity in the Z-direction

x = dimensional coordinate in cross-sectional plane parallel to the radius of curvature

X = dimensionless coordinate $= x/a$

y = dimensional coordinate in cross-sectional plane perpendicular to the radius of curvature

Y = dimensionless coordinate $= y/\lambda a$

z = curved spatial coordinate along tube center line

Z = dimensionless coordinate z/a

Greek Letters

λ = a parameter $= b/a$

μ = fluid viscosity

ν = fluid kinematic viscosity $= \mu/\rho$

ρ = fluid density

ψ = dimensionless stream function

ΔP_D = diametrical pressure drop, from the outer wall to the inner wall of the helix, measured along $Y = 0$

LITERATURE CITED

Austin, L. R., and J. D. Seader, "Fully Developed Viscous Flow in Coiled Circular Pipes," *AIChE J.*, **19**, 85 (1973).

Carre, B. A., "The Determination of Optimum Accelerating Factor for Successive Over-relaxation," *Computer J.*, **4**, 73 (1961).

Cuming, H. G., "Secondary Flow in Curved Pipes," Aeron. Research Council Reports and Memoranda No. 2880 (1952).

Dean, W. R., "Note on the Motion of Fluid in Curved Pipes," *Phil. Mag.*, **4** (7), 208 (1927).

———., "The Streamline Motion of Fluid in a Curved Pipe," *ibid.*, **5** (7), 673 1928).

Dufort, E. C., and S. P. Frankel, "Stability Conditions in the Numerical Treatment of Parabolic Differential Equations," *Math. Tables and Other Aids to Computation*, **7**, 135 (1953).

Eustice, J., "Experiments on Streamline Motion in Curved Pipes," *Proc. Royal Soc., Ser. A*, **85**, 119 (1911).

Joseph, B., "Numerical Treatment of Laminar Flow in Stationary and Oscillating Helical Coils of Square Cross-section," M.S. thesis, Case Western Reserve Univ., Cleveland, Ohio (1974).

Koutsky, J. A., and R. J. Adler, "Minimization of Axial Dispersion by Use of Secondary Flow in Helical Tubes," *Can. J. Chem. Eng.*, **42**, 239 (1964).

Price, H. S., R. S. Varga, and J. E. Warren, "Application of Oscillation Matrices to Diffusion Convection Equations," *J. Math. Physics*, **45**, 301 (1966).

Taylor, G. I., "The Criterion for Turbulence in Curved Pipes," *Proc. Royal Soc., Ser. A*, **124**, 243 (1929).
Truesdell, L. C. Jr., and R. J. Adler, "Numerical Treatment of Fully Developed Laminar Flow in Helically Coiled Tubes," *AIChE J.*, **16**, 1010 (1970).
White, C. M., "Stream-Line Flow Through Curved Pipes," *Proc. Royal Soc.*, **A123**, 645 (1929).
Young, D. M., "Iterative Methods for Solving Partial Differential Equations of Elliptic Type," *Trans. Am. Math. Soc.*, **76**, 92 (1954).

Supplementary material has been deposited as Document No. 02671 with the National Auxiliary Publications Service (NAPS), Microfiche Publications, 440 Park Ave. South, New York, NY 10016, and may be obtained for $1.50 for microfiche or $5.00 for photocopies.

Manuscript received May 8, 1974; revision received February 12 and accepted April 2, 1975.

Part II. Oscillating Helically Coiled Tubes

B. JOSEPH
and
R. J. ADLER

Chemical Engineering Department
Case Institute of Technology
Case Western Reserve University
Cleveland, Ohio 44106

The numerical method of Part I is extended to study periodic laminar flow in helically coiled tubes of square cross section oscillating sinusoidally about their helix axis. Depending on the relative strength of the wall velocity and the velocity of flow through the tube, one of three flow regimes occur. When the wall velocity is small, the computed results resemble these for a stationary helix. When the wall velocity dominates, the direction of the secondary flow is reversed. When the wall and flow velocities are comparable, the secondary flow pattern varies periodically in time and sometimes alternates in direction.

SCOPE

This part explores fluid flow in helically coiled tubes of square cross section oscillating about their helix axis. The fluid near the wall is dragged back and forth by wall motion. When the wall velocity is larger than the flow velocity, the fluid near the wall experiences larger centrifugal forces than the interior fluid and is thus thrown outward, away from the helix axis. Replacement fluid flows inward through the center of the cross section. The resulting twin counterrotating vortices resemble those found in secondary flow in stationary helically coiled tubes (see Part I), but the rotation is in the opposite direction. These wall motion induced secondary flows can be very strong.

Helically coiled tubes oscillating about their helix axis have been proposed by Bartlett and Drinker et al. (1969) as blood oxygenators. Experiments show high rates of oxygen transfer across tube walls made for semipermeable silicone membranes into blood. Cross-sectional mixing by strong secondary flows induced by the wall motion substantially eliminated mass transfer resistance within the blood. Moss (1971) attempted by correlate friction factors and mass transfer rates based on an approximate analysis. Another proposed application is an inertia type of pump (Fisher, 1959-1963). The authors of this paper believe there are additional potential applications such as continuous blenders, continuous polymerization reactors, and continuous centrifuges.

The objective of this study is to use numerical methods to survey the interaction of flow through helically coiled tubes caused by a constant pressure or constant flow driving force and the oscillation of the helically coiled tubes. The seven cases studied vary the flow for a constant radius of curvature and frequency of oscillation.

CONCLUSIONS AND SIGNIFICANCE

The computed solutions confirm that oscillating a helically coiled tube about its mandrel axis can induce strong secondary flows. Three flow regimes can be distinguished. When the maximum velocity of the oscillating tube wall is small compared to the velocity of flow through the tube, the effect of the oscillation is to reduce the strength of the secondary flow associated with flow through stationary helically coiled tubes. When the wall velocities are comparable to the flow velocity, the secondary flow varies periodically with time, sometimes changing direction during the oscillation. When the wall velocities are large compared to the flow velocity, there are two strong counterrotating vortices in the cross section, rotating opposite in direction to those observed in stationary helically coiled tubes.

Numerical methods are judged practical for calculating flow solutions for oscillating helically coiled tubes, at least over the range of variables studied in this work; solutions required three to four min. of computer time (Univac 1108).

The results reported here, together with prior studies of others, give a more detailed and systematic picture of fluid flow in oscillating helically coiled tubes than has been available heretofore. It is hoped that the additional background will encourage further investigations and uses of oscillating helically coiled tubes for process applications (see Scope).

Correspondence concerning this paper should be addressed to R. J. Adler.